

Optimized correlations inspired by perturbation theory

Martin Panholzer,^{1,2} Raphael Hobbiger,¹ and Helga Böhm¹

¹*Institute for Theoretical Physics, Johannes Kepler University Linz, Austria*

²*European Theoretical Spectroscopy Facility (ETSF)*

(Dated: February 11, 2021)

We study the accuracy of analytical wave function based many-body methods derived by energy minimization of a Jastrow-Feenberg ansatz for electrons (‘Fermi hypernetted chain approach’). Approximations to avoid the complexity of the fermion problem are chosen to parallel successful boson theories and be computationally efficient. For the three-dimensional homogeneous electron gas, we calculate the correlation energy and pair distribution function in comparison with simulation results. We also present a new variant of theory, compatible with the ladder sum of conventional perturbation theory, which performs particularly well in the highly dilute density regime.

I. INTRODUCTION

The quantum many body (MB) problem, a numerically hard problem, cannot be solved straightforwardly. Various different and competing approaches exist to approximate the solution, raising the question of finding the best method for a particular system. For an optimal choice, a thorough understanding is necessary of how the physics manifests itself in the theory. Here, we combine experience from three different successful fields, quantum Monte Carlo (MC), perturbation theory (PT), and the variational Jastrow-Feenberg (JF) approach. Refined JF versions have been developed for hard-core quantum fluids^{1,2}. We here aim at a better understanding of why different approximations perform differently, depending on the system parameters. In this context, the homogeneous electron gas (HEG) is of particular interest because, i) it is the most relevant model system for electronic structure methods, ii) well studied with various methods in its entire density range, and iii) the random phase approximation (RPA), often the starting point of PT, is well defined. In contrast, the bare RPA diverges for hard core potentials.

Monte Carlo methods, state-of-the-art for ground state computations, yield benchmark results for the energy³, the pair distribution function^{4,5} or the static density-density response function⁶. Extending their applicability range to excited states is an active research field, but the numerical demands remain extremely high^{7,8}.

Based on Feynman diagrams⁹, PT is another proven systematic attempt to treat MB systems. Most widely used for calculating excited state properties^{10,11}, it is also applied to the ground state^{12,13}. Practical implementations allow to retain only specific classes of diagrams, chosen according to the given situation. A prime example is the importance of self-energy graphs for quasiparticle properties^{11,14}. Another class arises from the Bethe-Salpeter equation (BSE), relevant for correct results on exciton binding observed by optical absorption^{10,15,16}.

Wave function based methods, finally, include physical intuition right from the start, either via a particular parametrization or a general functional form. We discuss fermions with only a distance-dependent interac-

tion $v(r)$, but the results could be generalized to, e.g., a dipolar interaction¹⁷ or lattice models¹⁸. An excellent choice is the JF-Slater wave function, $\psi = F\phi_0$; for homogeneous cases ϕ_0 is a plane wave Slater determinant, and $F = \prod_{i,j} f(|r_i - r_j|)$ with $f(r) = \exp(u_2(r))$ accounts for correlations¹⁹. The approach develops its full power when $u_2(r)$ is optimally determined via functional variation. Cluster expansions developed for classical liquids²⁰ inspired the extension of these techniques to quantum fluids²¹. The diagrams for the pair distribution function $g(r)$ are classified according to the Hyper Netted Chain (HNC) formalism²⁰, termed FHNC in its fermion version^{2,22–25}. Minimization of the energy determines the optimal u_2 and, consequently, g .

From a bird’s eye view, the full diagrammatic formalism²⁶ exactly maps u_2 to observables as illustrated in fig. 1 (left part). While some ingredients are obtained easily, the so-called elementary diagrams are arbitrarily difficult (similar to PT, where vertex corrections are complicated). If all diagrams could be summed exactly, the result with the optimal correlation function u_2 obtained from the Ritz principle (fig. 1, right), would essentially equal that of variational MC (VMC) with a parametrized u_2 that allows to reach the functional result.

The theory, as any, relies on approximations. Although not reaching quite the accuracy of the MC energies, FHNC-EL is numerically by orders of magnitude less demanding.²⁷ It thus allows a highly efficient evaluation of observables in a multi-variable space, like quantities depending on position r , density ρ , spin σ , and maybe valley indices²⁸. Most important, the FHNC can be systematically improved by topping it with PT, termed ‘correlated basis functions’ approach (CBF)²⁹. For the ground state this is comparable with stepping from VMC to released node diffusion MC. The CBF route is also the prime tool to extended the ground state theory to excited states^{30–35}. Again, in terms of accuracy versus computation time, obtaining dynamic properties via FHNC+CBF is much more efficient than by MC^{8,34}.

At first sight, PT and optimized JF wave functions appear very different. Their link for bosons was demonstrated by Jackson et al.^{36,37}, who showed which approximation to the sum of parquet diagrams leads to the

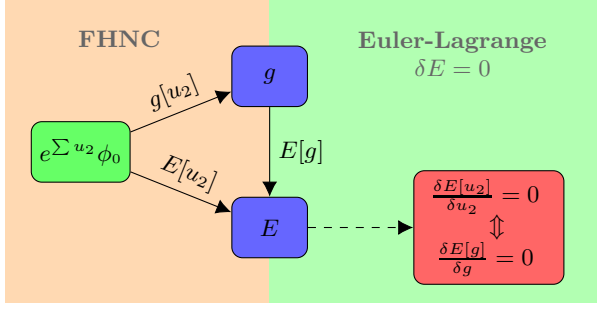


FIG. 1. Left: Graphical expansions provide an exact map from the JF correlations u_2 to the observables $g[u_2]$ (pair distribution function) and $E[u_2]$ (energy). Right: The optimal u_2 minimizes E , yielding the EL equation. This can equivalently be interpreted as a pair density functional theory.

HNC-EL equations. The purpose of this work is twofold: Firstly, we extend their studies to fermions. We derive a formulation, which is valid for highly dilute HEGs ($r_s > 5$, with the density $\rho = 3/4\pi(a_0 r_s)^3$, and effective Bohr radius a_0). Secondly, we here demonstrate that FHNC-EL variants^{2,24} perform very well even in their most basic version. They are easier to implement numerically than the more often employed approach of Singwi et al.³⁸ (STLS), give better results, and, additionally, yield more information on the effective interaction.

II. THEORY

In practical applications the series of elementary diagrams are approximated by different schemes, dependent on the considered system, to quantitatively improve the results. As we are aiming at a puristic form of the theory all elementary contributions are neglected, noting that they can be included in the presented derivation without much difficulty. Classically, this gives two HNC/0 equations which are solved self-consistently, one of them being algebraic in direct, the other one in reciprocal space. In the bosonic HNC/0-EL, the functional variation of the energy brings a differential ('Euler-Lagrange') equation into play, which takes the form of a Schrödinger equation for the short-range structure $\sqrt{g(r)}$.

Pursuing the same route for fermions makes the theory much more cumbersome. Exchange effects cause additional diagrams with more complex rules. The final result, FHNC/0-EL, is a set of eight plus eight coupled equations in direct and reciprocal space.

Due to the intricacy of the problem it is difficult to identify the FHNC-expressions with their corresponding parquet diagrams^{36,37}. A promising route suggested by Krotscheck², termed 'sFHNC', was to ensure the correct long wavelength limit, where the EL-equation is understood as the sum of ring diagrams (for more details cf. appendix A).

In contrast to that approach, routed in approximating the static structure factor $S(q)$ (q being the wave vec-

tor), we here derive a *real space* formulation, arriving at the boson parquet sum³⁷, where the ladder equation is supplemented by a correction for Fermi statistics. We denote this as 'ladder⁺ approach'.

The Slater exchange function $\ell(rk_F)$, i.e. the density matrix of the ϕ_0 determinant of a system with Fermi momentum $\hbar k_F$ and degeneracy factor ν determines the non-interacting $g_F(r) = 1 - \ell^2(rk_F)/\nu$, accounting for the Pauli exclusion hole. We start with the approximate FHNC expression for the pair distribution function,

$$g(r) = [1 + \Gamma(r)] g_F(r), \quad (1)$$

where correlation corrections to g_F are neglected.²³ Γ is determined by the nodal diagrams N

$$\Gamma(r) = \exp[u_2(r) + N(r)] - 1. \quad (2)$$

With these definitions the derivation is straightforwardly done by energy minimization. Note that an explicit expression for N is not needed here.

The energy per particle in the JF correlated ground state is obtained from the Hamiltonian per particle \hat{h} as²

$$\langle \psi | \hat{h} | \psi \rangle = t_0 + \frac{\rho}{2} \int d^3r g(r) V_{JF}(r) + t_{JF}, \quad (3a)$$

$$V_{JF}(r) = v(r) - \frac{\hbar^2}{4m} \nabla^2 u_2(r), \quad (3b)$$

where $t_0 \equiv \frac{3}{5} \frac{\hbar^2 k_F^2}{2m}$, and V_{JF} is called JF interaction (m denotes the particles' mass). The last term is

$$t_{JF} = \frac{\hbar^2 \rho}{8m\nu} \int d^3r \Gamma(r) \nabla^2 \ell^2(rk_F) + \mathcal{O}(\Gamma^2), \quad (3c)$$

where we only keep the leading order in Γ . Requiring the variation of the energy with respect to u_2 to vanish leads to the Euler-Lagrange equation

$$\frac{\hbar^2}{4m} \nabla^2 g(r) = \int d^3\bar{r} V_{JF}(\bar{r}) \frac{\delta g(\bar{r})}{\delta u_2(r)} + \frac{2}{\rho} \frac{\delta t_{JF}}{\delta u_2(r)}. \quad (4)$$

How the functional derivative is done is demonstrated by the first term on the right. First, g is replaced by eq. (1), where eq. (2) is inserted:

$$\int d^3\bar{r} V_{JF}(\bar{r}) \frac{\delta g(\bar{r})}{\delta u_2(r)} = g(r) (V_{JF}(r) + N'(r)) \quad (5a)$$

$$N'(r) \equiv \int d^3\bar{r} V_{JF}(\bar{r}) \frac{\delta N(r)}{\delta u_2(\bar{r})}. \quad (5b)$$

Here the Schwarz theorem generalized to functionals,

$$\frac{\delta g(\bar{r})}{\delta u_2(r)} = \frac{\delta g(r)}{\delta u_2(\bar{r})}, \quad (6)$$

was used. The last part of eq. (4) is treated analogously. The term analogous to N' , with V_{JF} replaced by $\nabla^2 \ell^2$, is neglected, being small compared to the former.³⁹

Finally, u_2 is eliminated in favor of g with eq. (2) and the identity

$$\nabla^2 g + g \nabla^2 \ln g = 4\sqrt{g} \nabla^2 \sqrt{g}. \quad (7)$$

The result takes the form of a Schrödinger equation,

$$\left[-\frac{\hbar^2}{m} \nabla^2 + v(r) + w_I(r) + \frac{\hbar^2 \nabla^2 \sqrt{g_F(r)}}{m \sqrt{g_F(r)}} \right] \sqrt{g(r)} = 0, \quad (8)$$

$$w_I(r) \equiv \frac{\hbar^2}{4m} \nabla^2 N(r) + N'(r). \quad (9)$$

The interpretation of eq. (8) is straightforward. An effective interaction $w_I(r)$ needs to be added to the bare interaction $v(r)$, supplemented with a correction due to the fermion propagator. The latter coincides with the exchange correction postulated by Kallio and Piilo²⁴.

So far, $w_I(r)$ is defined via the nodal diagrams. One can derive an expression from the diagrammatic formalism consistent with our starting point, eq. (1). While further improving $g(r \rightarrow 0)$, such an attempt does not change the long wavelength behavior. Since the cusp condition⁴⁰ is fulfilled, given that $w_I(r)$ is finite at the origin, we instead choose to incorporate the relevant $q \rightarrow 0$ terms by using the sFHNC expression for $w_I(r)$ as derived by Krotscheck²,

$$\tilde{w}_I(q) = -\frac{\hbar^2 q^2}{4m} \left[\frac{1}{S(q)} - \frac{1}{S_F(q)} \right]^2 \left[2 \frac{S(q)}{S_F(q)} + 1 \right], \quad (10)$$

with S_F being the free static structure factor. Equations (8) and (10) constitute a closed set of equations to be solved self-consistently. Note that the non-interacting limit is correctly reproduced. Remarks on the implementation are given in appendix B.

Before we present numerical results, we clarify the physics contained in the potential w_I by establishing the relation to its bosonic counterpart. Setting $g_F = 1$, $V \equiv v + w_I$, and $L \equiv -\frac{\hbar^2}{m} \nabla^2 (\sqrt{g} - 1)$, eq. (8) reads in real and in Fourier space

$$\left[-\frac{\hbar^2}{m} \nabla^2 + V(r) \right] (\sqrt{g(r)} - 1) + V(r) = 0, \\ \tilde{L}(q) = \tilde{V}(q) + \int \frac{d^3 k}{(2\pi)^3} \tilde{V}(\mathbf{q} - \mathbf{k}) \frac{\tilde{L}(k)}{t(k)}. \quad (11)$$

This is recognized as the Bethe-Goldstone equation⁴¹. The similarity is no coincidence, as our derivation parallels that including the ladders in boson parquet theory³⁷ and, indeed, w_I can be identified with the particle-particle irreducible interaction. We denote the approach with w_I of eq. (10) as ladder⁺ approximation, to emphasize that it self-consistently sums ladders and bubbles. The crucial point here is that eq. (3) is a better approximation to the ladders as compared to eq. (A1) of appendix A, which is superior for the bubble diagrams. Which precise approximations in PT lead to the

EL eq. (8) remains open. Nevertheless, as a result derived from an alternative formalism it can give new hints and thus open the door for new approximation schemes in PT (in this particular case for ladder sums). How to treat which diagrams is often founded mainly on experience and hard to motivate from PT alone.

III. RESULTS

We now test the ladder⁺ approach by applying it to the HEG. The basic assessment of a theory's accuracy is to compare the correlation energy per particle, $e_c(r_s)$, with simulation results. We obtain it by coupling constant integration from the pair distribution function $g_{r_s}(r)$ at a density given by r_s

$$e_c(r_s) = \frac{1}{2r_s^2} \int_0^{r_s} d\tilde{r}_s \frac{3}{4\pi\tilde{r}_s^2} \int d^3 r v(r) (g_{\tilde{r}_s}(r) - g_F(r)). \quad (12)$$

The correlation energy in the ladder⁺ and the sFHNC approximation of FHNC-EL theory are compared to MC results in fig. 2. It is seen that the sFHNC works well for metallic densities (how the deviation for $r_s \rightarrow 0$ can be corrected is reported in appendix A). In accordance with the findings of PT that the summation of ladder diagrams is crucial in the highly correlated regime⁴¹, the ladder⁺ curve is essentially indistinguishable from the MC reference for low densities. Another important FHNC-EL is that of Kallio et al.²⁴, derived from the bosonic HNC-EL by enforcing the non-interacting fermion limit. For brevity, we call it bFHNC. Although less rigorous in derivation, it performs very well over the whole r_s range. Only for extremely low and for high densities the respective PT inspired approximations are superior.

Despite the substantial simplifications of the various propagators in the three FHNC approaches, they perform notably well. This indicates that their effective interactions are of high quality, accounting for the most relevant physics in each density regime. We also compare to the best available numerical BSE results, obtained recently by Maggio and Kresse¹³. They evaluated the four-point particle-hole ladders with a static RPA screened interaction. It appears promising to replace this by FHNC (CBF) interactions, for the particle-hole ladder³² derived in Ref.44.

An accurate energy does not guarantee a high quality wave function or structure factor in the same approximation. As is well known, the STLS³⁸ yields excellent correlation energies, but fails for $g(r \rightarrow 0)$, yielding unphysical negative values for $r_s \gtrsim 4$. The pair distribution functions at $r_s = 5$ are displayed in fig. 3. The sFHNC and STLS clearly deviate from the MC data (we show the most recent simulations of Spink et al.⁵). Remarkably, the ladder⁺ approximation is now closer to MC than the bFHNC, which worked best for e_c . We conclude that $g(r)$ is most satisfying in ladder⁺, but the kinetic energy is less accurate. Equivalently stated, the error in e_c

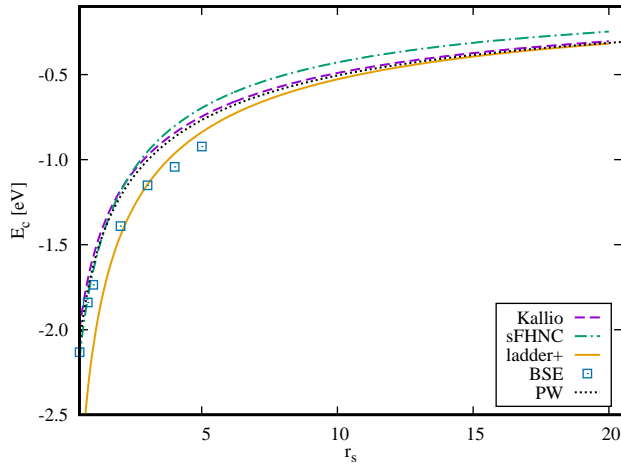


FIG. 2. Correlation energy per particle versus density parameter. Three FHNC variants, the bFHNC of Kallio et al.²⁴ (dashed violet line), Krotscheck's² sFHNC bubble-summation (dot-dashed cyan line) and the ladder⁺ approach (full orange line) are compared to BSE¹³ (boxes) and parametrized⁴² MC data⁴³ (dotted black line).

is carried over by the coupling constant integration (12) from the inadequate small r_s performance. This trend continues to higher r_s values and also for the fully spin polarized HEG, depicted in fig. 4, again for $r_s = 5$. For small r the spin polarized ladder⁺ result is on top of the MC benchmark curve⁵.

An interesting question concerns the position r_{m1} of the first peak in $g(r)$, foreshadowing the Wigner crystal's nearest neighbor position. The MC peak has lowest r_{m1} , for the paramagnetic HEG in close agreement with bFHNC and ladder⁺. The ferromagnetic first maximum is too far right in ladder⁺, indicating that $w_I(q \rightarrow 0)$ needs some improvement with respect to the S_F -terms. The sFHNC peak is too low.

Note that these discrepancies are tiny ($\sim 2\%$). For the two-dimensional (2D) HEG, where correlation effects are more pronounced, the neglect of elementary diagrams and triplet correlations will lead to larger deviations, the partially spin-polarized case⁴⁵ being under investigation (in 3D cf. Davoudi *et al.*²⁵). This trend continues in the 1D case, but still being a reasonable starting point^{46,47}.

Of course, some of the less satisfactory features of the above approaches can be removed: For the STLS a scheme was suggested by Takada⁴⁸, in sFHNC $g(r) > 0$ can be enforced by exponential mixing in the iteration steps. However, we here want to compare them in their 'most naked' form and it turns out that even these FHNC versions perform highly satisfactory.

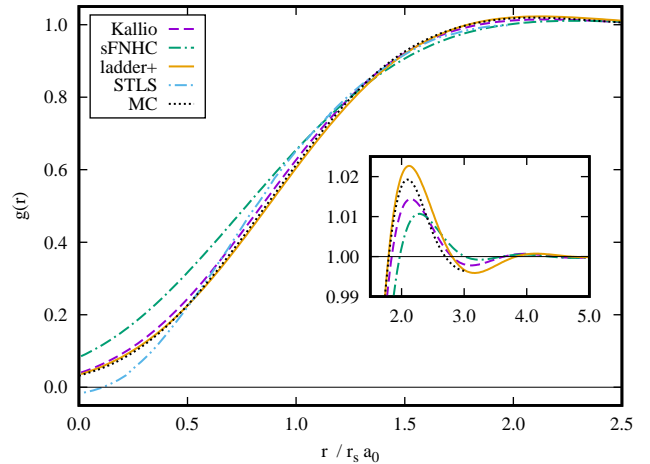


FIG. 3. Pair distribution function for the paramagnetic HEG at $r_s = 5$ in the ladder⁺, bFHNC²⁴ and sFHNC² approaches (line types as in fig. 2), compared to a fit of MC data by Spink et al.⁵ (dotted black curve). The STLS³⁸ (double-dot-dashed light blue line). The inset shows the first maximum.

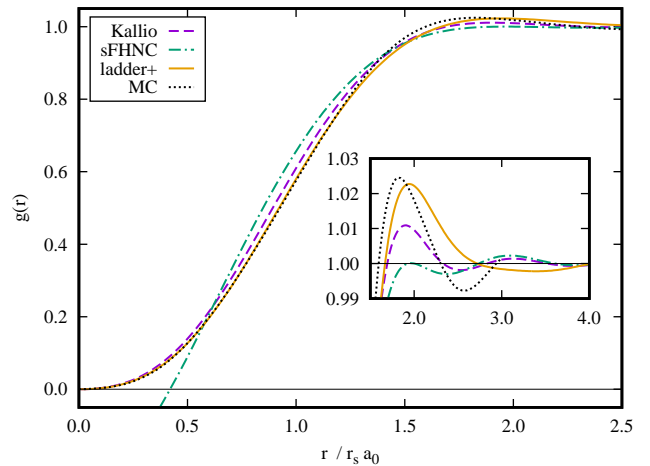


FIG. 4. Same as fig. 3, but for the ferromagnetic HEG. The STLS curve was omitted, lying significantly below the sFHNC.

IV. CONCLUSION

We here demonstrated the strength of uncomplicated FHNC-EL versions. Their key advantage is to be based on *functional* optimization, thus yielding a parameter-free, unbiased result for the ground state structure. The intricacy of the full fermion version is avoided neglecting elementary diagrams and correlation corrections to g_F . The resulting self-consistency equations exhibit physical transparency and share the low computational demand with classical HNC. From a practical perspective, they are thus extremely efficient, while nevertheless yielding rather accurate results.

The HEG served as our test-system for comparing the following specific approaches: the bFHNC presented by Kallio and Piilo²⁴ for electrons and the sFHNC introduced by Krotscheck². We further developed a new FHNC-EL version, particularly suited for the short range region of soft potentials and the low density limit of HEGs. Like the sFHNC, it self-consistently sums approximated ladder and bubble diagrams with emphasis on the former, motivating the term ladder⁺ approach.

The bFHNC method performs best in a wide density range, yielding both, pair distribution function and correlation energy close to the MC benchmark data. For high and low densities, $g(r)$ is more accurate in sFHNC and ladder⁺, respectively. These versions have the additional advantage to allow a better connection with PT. Consequently, their extension to inhomogeneous, in particular periodic systems⁴⁷, holds a high potential for an implementation in combination with PT algorithms, e.g. in BSE¹³ for solid state physics applications.

Apart from the good performance combined with the very low numerical demand the following needs to be stressed: The derivations in the FHNC-EL formalism are intricate, but they *justify* the resulting equations and functionals. Once established, these energy functionals can be applied in a pair density functional theory^{25,49–51}, the pair analog of density functional theory.

Finally, the possibility of coherently refining the method via CBF and generalizing the static ground state correlations to dynamic fluctuations^{31,33} underpins the value and utility of the FHNC approach.

The research was supported by the Austrian science Fund FWF under Project No. J 3855-N27.

Appendix A: sFHNC

We provide a brief summary of the sFHNC as formulated by Krotscheck². The static structure factor S and its non-interacting counterpart S_F are related to the sum of all direct-direct cluster diagrams $\Gamma \equiv \Gamma_{dd}$ via

$$S(q) = S_F(q) (1 + S_F(q) \tilde{\Gamma}(q)), \quad (\text{A1})$$

which is exact for long wavelengths. The correlation function u_2 in eq. (2) is optimally determined from minimizing the ground state energy. Denoting the energy of a free particle as $t(q) \equiv \hbar^2 q^2 / 2m$, the resulting EL equation reads

$$S(q) = \frac{S_F(q)}{\sqrt{1 + \frac{2S_F^2(q)}{t(q)} \tilde{V}_{ph}(q)}}, \quad (\text{A2})$$

where the ‘particle-hole potential’ V_{ph} (more precisely, the particle-hole irreducible interaction²) is given by

$$V_{ph}(r) = (1 + \Gamma(r)) v(r) + \frac{\hbar^2}{m} \left| \sqrt{1 + \Gamma(r)} \right|^2 + \Gamma(r) w_I(r). \quad (\text{A3})$$

Here, w_I is related to the summed nodal diagrams exactly as in (9). Consistent with the approximations leading to (A1), it can be expressed in terms of the static structure function, resulting again in eq. (10). From $\Gamma(r)$ the potential V_{ph} is obtained with (A3), yielding $S(q)$ via (A2), and then Γ for the next iteration step from (A1).

We emphasize, that the sFHNC contains both, rings and also ladder diagrams in V_{ph} given in (A3), summed in an approximate but consistent way. The theory is designed to exactly reproduce the FHNC $q \rightarrow 0$ limit.

If all elementary diagrams are taken into account, the direct- and reciprocal-space formulations of FHNC-EL are equivalent. Therefore, when neglecting them in any finite order n in FHNC/ n -EL, a consistent choice between the sFHNC and ladder⁺ approximation has to be made. A possibility to resolve this inconsistency has been made in FHNC/C-EL²³ by interpolating the long and short wavelength limit.

From a dynamic perspective, the density response function $\chi(q, \omega)$ defines a dynamic effective interaction via $\chi = \chi^0 / (1 - \tilde{V}_{eff} \chi^0)$, where χ^0 is the non-interacting polarizability⁹. The use of a static \tilde{V}_{eff} generates the ring (= ‘bubble’) diagrams⁵². Approximating additionally χ^0 by a single pole (termed ‘collective approximation’, CA),

$$\chi_0^{CA}(q, \omega) = \frac{2t(q)}{(\omega + i\eta)^2 - (t(q) S_F(q))^2} \quad (\text{A4})$$

yields the ‘plasmon pole approximation’ for χ and conserves the m_1 (or f-)sum rule. In addition, the fluctuation-dissipation theorem (or m_0 sum rule) reproduces (A2).

If the final self-consistent $\tilde{V}_{ph}(q)$ from the sFHNC is inserted as $\tilde{V}_{eff}(q)$ into $\chi(q, \omega)$ *without* the CA, this gives an $S(q)$ somewhat different from eq. (A2). Krotscheck^{2,29} showed that this ‘CBF-correction’ structure factor reproduces the MC correlation energies also for $r_s \rightarrow 0$. As was pointed out early^{22,23}, the JF theory yields an error of 8% for $e_c(r_s \rightarrow 0)$ also in more elaborate versions with elementary diagrams and higher order correlations u_n . This is due to their state-independence (a local u_2 , depending only on a single variable r , cannot fully account for the momentum correlations between two ground-state fermions). Per construction, the JF ansatz aims at an improved treatment of strongly correlated systems, the $r_s \rightarrow \infty$ limit can easily be obtained with other means. The error decreases rapidly with increasing correlation. But in case of need, CBF provides a powerful method to extend the accuracy of FHNC-EL to weak correlations.

Appendix B: Implementation

We here show a favorable procedure to treat the set of equations (8) and (10). Instead of numerically solving the differential equation (8) directly, a straightforward manipulation maps it onto a simple algebraic equation

in reciprocal space. By adding the bosonic interaction

$$\tilde{w}_{\text{IB}}(q) \equiv -\frac{\hbar^2 q^2}{4m} \left[\frac{1}{S(q)} - 1 \right]^2 [2S(q) + 1] \quad (\text{B1})$$

to (8), we can write the static structure factor as

$$S(q) = \frac{1}{\sqrt{1 + \frac{2}{t(q)} \tilde{V}_{\text{aux}}(q)}}, \quad (\text{B2})$$

where the auxiliary potential reads in real space

$$V_{\text{aux}}(r) = \left[v(r) + w_{\text{I}}(r) + \frac{\hbar^2 \nabla^2 \sqrt{g_{\text{F}}(r)}}{m \sqrt{g_{\text{F}}(r)}} \right] g(r) - w_{\text{IB}}(r) + \frac{\hbar^2}{m} |\nabla \sqrt{g(r)}|^2. \quad (\text{B3})$$

An initial guess for $g(r)$ gives an auxiliary potential $V_{\text{aux}}(r)$ from (B3) and in turn, after a Fourier transform (FT), where we use the following convention

$$\tilde{V}_{\text{aux}}(q) = \rho \int d^3r e^{-i\mathbf{q}\cdot\mathbf{r}} V_{\text{aux}}(r) \quad (\text{B4a})$$

a static structure factor from (B2). The inverse FT gives a new $g(r)$ from

$$g(r) - 1 = \int \frac{d^3q}{(2\pi)^3 \rho} e^{i\mathbf{q}\cdot\mathbf{r}} (S(q) - 1). \quad (\text{B4b})$$

These equations are iterated until convergence is achieved, merely having the FT as rate limiting step. Note that in contrast to methods of the STLS type³⁸, the here presented FHNC-EL approaches are easier to implement as no integration is necessary.

An implementation of all three versions discussed here, the sFHNC, the bFHNC and the ladder⁺ method can be found at https://github.com/mpanho/FHNC_3D.git.

-
- ¹ A. Fabrocini, S. Fantoni, and E. Krotschek, *Introduction to modern methods of quantum many-body theory and their Applications*, Series on Advances in Quantum Many-Body Theory, Vol. 7 (World Scientific, 2002) p. 413.
 - ² E. Krotschek, J. Low Temp. Phys. **119**, 103 (2000).
 - ³ G. Ortiz, M. Harris, and P. Ballone, Phys. Rev. Lett. **82**, 5317 (1999).
 - ⁴ P. Gori-Giorgi, F. Sacchetti, and G. Bachelet, Phys. Rev. B **61**, 7353 (2000).
 - ⁵ G. G. Spink, R. J. Needs, and N. D. Drummond, Phys. Rev. B **88**, 085121 (2013).
 - ⁶ S. Moroni, D. M. Ceperley, and G. Senatore, Phys. Rev. Lett. **75**, 6 (1995).
 - ⁷ M. Motta, D. E. Galli, S. Moroni, and E. Vitali, J. Chem. Phys. **143**, 164108 (2015).
 - ⁸ M. Nava, D. E. Galli, S. Moroni, and E. Vitali, Phys. Rev. B **87**, 1 (2013).
 - ⁹ A. L. Fetter and J. D. Walecka, *Quantum Theory of Many-Particle Systems* (Mc Graw-Hill, 1971).
 - ¹⁰ M. Rohlfing and S. G. Louie, Phys. Rev. B **62**, 4927 (2000).
 - ¹¹ G. Onida, L. Reining, and A. Rubio, Rev. Mod. Phys. **74** (2002).
 - ¹² B. Holm and F. Aryasetiawan, Phys. Rev. B **62**, 4858 (2000).
 - ¹³ E. Maggio and G. Kresse, Phys. Rev. B **235113**, 1 (2016).
 - ¹⁴ F. Aryasetiawan and O. Gunnarsson, Reports Prog. Phys. **61**, 237 (1998).
 - ¹⁵ S. Albrecht, L. Reining, R. Del Sole, and G. Onida, Phys. Rev. Lett. **80**, 4510 (1998).
 - ¹⁶ M. Gatti and F. Sottile, Phys. Rev. B **88**, 155113 (2013).
 - ¹⁷ A. Macia, D. Hufnagl, F. Mazzanti, J. Boronat, and R. E. Zillich, Phys. Rev. Lett. **109**, 235307 (2012).
 - ¹⁸ X. Q. G. Wang, S. Fantoni, E. Tosatti, and L. Yu, Phys. Rev. B **41** (1990).
 - ¹⁹ This is often a starting point for VMC calculations with a parametrized $u_2(r)$. For bosons, the JF form is exact, when correlations u_n are included to all orders.
 - ²⁰ J.-P. Hansen and I. R. McDonald, *Theory of simple liquids: with applications to soft matter* (2013) p. 619.
 - ²¹ A. Polls and F. Mazzanti, in ref. 1: Microscopic description of Quantum Liquids (2002) pp. 49–119.
 - ²² J. G. Zabolitzky, Phys. Rev. B **22**, 2353 (1980).
 - ²³ E. Krotschek, Ann. Phys. (N. Y). **155**, 1 (1984).
 - ²⁴ A. Kallio and J. Piilo, Phys. Rev. Lett. **77**, 4237 (1996).
 - ²⁵ B. Davoudi, R. Asgari, M. Polini, and M. P. Tosi, Phys. Rev. B **68**, 155112 (2003).
 - ²⁶ In the literature, ‘(F)HNC’ is used for both, the exact cluster expansion including all elementary diagrams, or the version where these are neglected (also termed ‘(F)HNC/0’).
 - ²⁷ The scaling for homogeneous systems is $n \log n$ for n sampling points of $g(r)$ in the FHNC/0-EL.
 - ²⁸ O. Gunawan, Y. P. Shkolnikov, K. Vakili, T. Gokmen, E. P. De Poortere, and M. Shayegan, Phys. Rev. Lett. **97**, 186404 (2006).
 - ²⁹ E. Krotschek, in ref. 1: Theory of Correlated Basis Functions.
 - ³⁰ H. Godfrin, M. Meschke, H.-J. Lauter, A. Sultan, H. M. Böhm, E. Krotschek, and M. Panholzer, Nature **483**, 576 (2012).
 - ³¹ H. M. Böhm, R. Holler, E. Krotschek, and M. Panholzer, Phys. Rev. B **82**, 224505 (2010).
 - ³² M. Panholzer, H. M. Böhm, R. Holler, and E. Krotschek, J. Low Temp. Phys. **158**, 135 (2010).
 - ³³ M. Panholzer, M. Gatti, and L. Reining, Phys. Rev. Lett. **120**, 166402 (2018).
 - ³⁴ G. E. Astrakharchik, R. E. Zillich, F. Mazzanti, and J. Boronat, Phys. Rev. A **94**, 063630 (2016).
 - ³⁵ E. Akaturk, S. H. Abedinpour, and B. Tanatar, Journal of Physics Communications **2**, 015018 (2018).
 - ³⁶ A. D. Jackson, A. Lande, and R. A. Smith, Phys. Rep. **86**, 55 (1982).

- ³⁷ A. D. Jackson, A. Lande, and R. A. Smith, Phys. Rev. Lett. **54** (1985).
- ³⁸ K. S. Singwi, M. P. Tosi, R. H. Land, and A. Sjölander, Phys. Rev. **176**, 589 (1968).
- ³⁹ Keeping this term doesn't alter the final form of the EL-equation, it simply modifies the induced interaction.
- ⁴⁰ J. C. Kimball, Phys. Rev. A **7**, 1648 (1973).
- ⁴¹ E. Lipparini, *Modern Many-Particle Physics* (World Scientific, 2003) p. 444.
- ⁴² J. P. Perdew and Y. Wang, Phys. Rev. B **45**, 13244 (1992).
- ⁴³ D. M. Ceperley and B. J. Alder, Phys. Rev. Lett. **45**, 566 (1980).
- ⁴⁴ M. Panholzer, *Pair excitations and exchange effects in the dynamics of strongly correlated Fermifluids*, Ph.D. thesis, Johannes Kepler University (2010).
- ⁴⁵ K. Dominik, S. Clemens, A. Katharina, and B. H. M., Contr. to Plasma Physics **58**, 179 (2018).
- ⁴⁶ R. Asgari, Solid State Commun. **141**, 563 (2007).
- ⁴⁷ M. Panholzer, J. Low Temp. Phys. **187**, 639 (2017).
- ⁴⁸ K. Yoshizawa and Y. Takada, Journal of Physics: Condensed Matter **21**, 064204 (2009).
- ⁴⁹ E. Krotscheck, Physics Letters A **190**, 201 (1994).
- ⁵⁰ F. Furche, Phys. Rev. A **70**, 022514 (2004).
- ⁵¹ M. Higuchi and K. Higuchi, Comput. Theor. Chem. **1003**, 91 (2013).
- ⁵² With the bare interaction, the conventional RPA is obtained.